



Testing dark energy models in the light of σ_8 tension

Gaetano Lambiase^{1,2,a}, Subhendra Mohanty^{3,b}, Ashish Narang^{3,4,c}, Priyank Parashari^{3,4,d}

¹ Dipartimento di Fisica “E.R. Caianiello”, Università di Salerno, 84084 Fisciano, SA, Italy

² INFN - Gruppo Collegato di Salerno, Fisciano, Italy

³ Theoretical Physics Division, Physical Research Laboratory, Ahmedabad 380009, India

⁴ Indian Institute of Technology, Gandhinagar, India

Received: 6 May 2018 / Accepted: 30 January 2019 / Published online: 15 February 2019

© The Author(s) 2019

Abstract It has been pointed out that there exists a tension in $\sigma_8 - \Omega_m$ measurement between CMB and LSS observation. In this paper we show that $\sigma_8 - \Omega_m$ observations can be used to test the dark energy theories. We study two models, (1) Hu–Sawicki (HS) Model of $f(R)$ gravity and (2) Chavallier–Polarski–Linder (CPL) parametrization of dynamical dark energy (DDE), both of which satisfy the constraints from supernovae. We compute σ_8 consistent with the parameters of these models. We find that the well known tension in σ_8 between Planck CMB and large scale structure (LSS) observations is (1) exacerbated in the HS model and (2) somewhat alleviated in the DDE model. We illustrate the importance of the σ_8 measurements for testing modified gravity models. Modified gravity models change the matter power spectrum at cluster scale which also depends upon the neutrino mass. We present the bound on neutrino mass in the HS and DDE model.

1 Introduction

The Λ CDM model is conventional paradigm which is invoked to explain the observations of CMB temperature anisotropy and matter power spectrum [1]. However it has been pointed out [2–8] that there is some discordance between CMB and LSS observations. Specifically, σ_8 , the r.m.s. fluctuation of density perturbations at $8 h^{-1}$ Mpc scale, inferred from Planck-CMB data and that from LSS observations do not agree. There have been many generalizations of the Λ CDM model to attempt the reconciliation between the two sets of results. For example, it has been shown that self interaction in dark matter-dark energy sector [9–14] and

several other scenarios [15–21] can reconcile the σ_8 tension. There is also a tension in the inference of Hubble constant H_0 from CMB observations and that determined from LSS observations [4]. The value of H_0 is also directly measured from Supernova-Ia (SN-Ia) observation (referred as local H_0) [22] which is also not in agreement with H_0 obtained from CMB observation (referred as local H_0 tension). The H_0 discrepancy between CMB and LSS observations can be resolved by including active massive neutrinos [4]. Whereas addition of a sterile massive neutrino helps resolving the local H_0 tension [23]. Varying the equation of state parameter w and effective number of relativistic degrees of freedom N_{eff} freely has also been shown to resolve the local H_0 tension [24–26]. Extended parameter space of Λ CDM model have also been shown to resolve local H_0 tension and σ_8 tension [27, 28]. It has been shown recently that both σ_8 and H_0 tension between CMB and LSS observations can be resolved simultaneously by invoking a viscous dark matter [29] and effective cosmological viscosity [30]. The bound on neutrino mass is also different in different models of cosmology [31–35].

The main conceptual problem with Λ CDM model is that there is no explanation of the origin and the unusually small value of the cosmological constant (Λ). One popular class of models which addresses this is the $f(R)$ gravity [36] models, in which the cosmological constant is generated dynamically from the curvature. We consider the Hu–Sawicki $f(R)$ gravity model which also satisfies the constraints from solar system tests [36]. One may also take a phenomenological approach of generalizing the cosmological constant to a dynamical variable and determine from observation how it changes in time. An example of this is the DDE model which avoids the problem of phantom crossing. For earlier works on cosmological parameter estimation with DDE models and $f(R)$ gravity models see [28, 37, 38].

^a e-mail: lambiase@sa.infn.it

^b e-mail: mohanty@prl.res.in

^c e-mail: ashish@prl.res.in

^d e-mail: parashari@prl.res.in

In this paper we explore the aspect of structure formation in HS Model and DDE model. In Hu–Sawicki model, we compute the power spectrum and constrain the parameters with Planck-CMB and LSS data. We find that the tension in σ_8 between Planck-CMB and LSS observations worsens in the HS model compared to the Λ CDM model. The second model we examine is DDE, non-phantom (equation of state $w \geq -1$) model of dark energy. We choose the values of two model parameters in this model such that the non-phantom condition is maintained and obtain σ_8 from Planck-CMB and LSS data sets. We find that in the DDE model the σ_8 tension is eased as compared to Λ CDM model.

Neutrino mass cuts the power at small length scales due to free streaming. The cosmology bound on neutrino mass changes in modified gravity models. We find that the constraint on neutrino mass $\sum m_\nu \leq 0.157$ in Λ CDM model changes to $\sum m_\nu \leq 0.318$ in the HS model and $\sum m_\nu \leq 0.116$ in the DDE model from CMB observations. Whereas, $\sum m_\nu = 0.364 \pm 0.095$ in Λ CDM model changes to $\sum m_\nu = 0.333 \pm 0.093$ in the HS model and $\sum m_\nu = 0.275 \pm 0.095$ in the DDE model from LSS observations. All these bounds are at 68% c.l. All these constraints are obtained considering that all three neutrinos have degenerate mass. We also check the H_0 inconsistency and find that it is being resolved on inclusion of neutrino mass in both these models, consistent with the earlier findings [4] that neutrino mass resolves the H_0 conflict.

The structure of this paper is as follows. In Sect. 2 we briefly discuss the Hu–Sawicki $f(R)$ model and the modification in the evolution equations. In Sect. 3 we describe the phenomenological parametrization of DDE model. We describe the role of massive neutrinos in cosmology and their evolution equations in Sect. 4. In Sect. 5 matter power spectrum and its relation to σ_8 has been discussed briefly. We also explain the effect of HS, DDE model parameters and massive neutrinos on the matter power spectrum in this section followed by the description of data sets used and analyses done in Sect. 6. We conclude with discussion in Sect. 7.

2 f(R) theory: Hu–Sawicki model

Scalar-tensor theories are generalized Brans–Dicke [39] theories. The general action for scalar-tensor theories is

$$S_{\text{st}} = \int d^4x \sqrt{-\tilde{g}} \left(\frac{\tilde{R}}{16\pi G} - \frac{1}{2} \tilde{g}^{\mu\nu} \partial_\mu \phi \partial_\nu \phi - V(\phi) \right) + S_m(g_{\mu\nu}, \psi), \tag{1}$$

where $S_m(g_{\mu\nu}, \psi)$ is the action for the matter fields, $g_{\mu\nu}$ is Jordan frame metric and $\tilde{g}_{\mu\nu}$ is Einstein frame metric which are related by the conformal transformation $g_{\mu\nu} = A^2(\phi)\tilde{g}_{\mu\nu}$, and ϕ is the scalar field which couples to Einstein

metric as well as to matter fields ψ . The scalar field brings in an additional gravitational interaction between matter fields and the net force on a test particle modifies to

$$\mathbf{F} = -\nabla\psi - \frac{d \ln A(\phi)}{d\phi} \nabla\phi, \tag{2}$$

and the dynamics is governed by the effective potential

$$V_{\text{eff}}(\phi) = V(\phi) + (A(\phi) - 1)\rho, \tag{3}$$

where Ψ is Newtonian potential and ρ is density.

The fact that scalar field couples to the matter fields would result in violations of the Einstein Equivalence Principle [40] and signatures of this coupling would appear in non-gravitational experiments based on universality of free fall and local Lorentz symmetry [41] in the matter sector. These experiments severely constrain the presence of a scalar field and can be satisfied if either the coupling of the scalar field with the matter field is always very small or there is some mechanism to hide this interaction in the dense environments. One such mechanism is called chameleon mechanism [42] in which $V(\phi)$ and $A(\phi)$ are chosen in such forms that $V_{\text{eff}}(\phi)$ has density dependent minimum, i.e., $V_{\text{eff}}(\phi)_{\text{min}} = V_{\text{eff}}(\phi(\rho))$. The required screening will be achieved if either the coupling is very small at the minimum of $V_{\text{eff}}(\phi)$ or the mass of the scalar field is extremely large.

If the scalar field stays at its density dependent minimum, $\phi(\rho)$, the theory can be parametrized into two functions, the mass function $m(\rho)$ and the coupling $\beta(\rho)$ at the minimum of the potential [43,44]

$$\frac{\phi(\rho) - \phi_c}{m_{\text{Pl}}} = \frac{1}{m_{\text{Pl}}^2} \int_\rho^{\rho_c} d\rho \frac{\beta(\rho)}{m^2(\rho)}, \tag{4}$$

where m_{Pl} is the Planck mass and mass of the scalar field $m(\rho)$ and the coupling parameter $\beta(\rho)$ are respectively given as

$$m^2(\rho) = \frac{d^2 V_{\text{eff}}}{d\phi^2} |_{\phi=\phi(\rho)}, \tag{5}$$

$$\beta(\rho) = m_{\text{Pl}} \frac{d \ln A}{d\phi} |_{\phi=\phi(\rho)}. \tag{6}$$

Simplest modified gravity model is the $f(R)$ gravity [45–47]. In general relativity (GR) Lagrangian density is given by Ricci scalar R , whereas it is a non linear function of R in the $f(R)$ gravity. Hence the action for an $f(R)$ theory is given as

$$S = \frac{1}{16\pi G} \int d^4x \sqrt{-g} (f(R)) + S_m(g_{\mu\nu}, \psi), \tag{7}$$

where $f(R)$ is a non linear function of R . The scalar degree of freedom in the $f(R)$ theories has been utilized as the

quintessence field to explain DE. It has been shown [46,48] that $f(R)$ theory is the equivalent to a scalar-tensor theory with an equivalence relation

$$f_R = e^{-2\beta_0\phi_R/m_{Pl}}, \tag{8}$$

and potential corresponding to extra scalar degree of freedom

$$V(\phi_R) = \frac{m_{Pl}^2}{2} \frac{Rf_R - f(R)}{f_R^2}, \tag{9}$$

where $f_R = \partial f/\partial R$. In this paper, we consider the Hu-Sawicki model, which explains DE while evading the stringent tests from solar system observations. In HS model the modification in the action is given as

$$f(R) = R - 2\Lambda - \frac{f_{R_0}}{n} \frac{R_0^{n+1}}{R^n}, \tag{10}$$

where $R \geq R_0$ and R_0 is the curvature at present. Here f_{R_0} and n are the free parameters of the HS model. Using equivalence relation 8 and Eq. 9, we find that

$$V(\phi_R) = \Lambda + \frac{n+1}{n} f_{R_0} R_0 \left(\frac{-2\beta_0\phi_R}{m_{Pl}f_{R_0}} \right)^{n/(n+1)} \tag{11}$$

The coupling function $\beta(a)$ is constant for all the $f(R)$ models *i.e* $\beta(a) = \frac{1}{\sqrt{6}}$, whereas the mass function is a model dependent quantity [43,44,49]. In particular for the HS model, for which form of $f(R)$ is given by Eq. 10, we have mass function

$$m(a) = m_0 \left(\frac{4\Omega_\Lambda + \Omega_m a^{-3}}{4\Omega_\Lambda + \Omega_m} \right)^{(n+2)/2}, \tag{12}$$

with

$$m_0 = H_0 \sqrt{\frac{4\Omega_\Lambda + \Omega_m}{(n+1)f_{R_0}}}, \tag{13}$$

These parameters contains all the information of the model, where Ω_Λ and Ω_m are the matter density fraction for dark energy and matter today. In the next subsection, we will derive the evolution equations in terms of these parameters.

2.1 Evolution equations

In GR the evolution of metric perturbation potentials and density perturbations is given by the following linearized equations,

$$k^2\Phi = -4\pi G a^2 \rho \delta, \tag{14}$$

$$k^2(\Phi - \Psi) = 12\pi G a^2 (\rho + P)\sigma, \tag{15}$$

$$\delta'' + \mathcal{H}\delta' - 4\pi G a^2 \rho \delta = 0, \tag{16}$$

where ' denotes the derivative with respect to the conformal time, δ is the co-moving density contrast and Φ and Ψ are the space-time dependent perturbations to the FRW metric,

$$ds^2 = -(1 + 2\Phi)dt^2 + a^2(t)(1 - 2\Psi)\delta_{ij}dx^i dx^j. \tag{17}$$

In the modified gravity models and other dark energy models these relation can be different. To incorporate the possible deviations from Λ CDM evolution there are several parametrization [50–54] present in the literature. We use the following parametrization which was introduced in [50]

$$k^2\Psi = -4\pi G a^2 \mu(k, a)\rho\delta, \tag{18}$$

$$\frac{\Phi}{\Psi} = \gamma(k, a), \tag{19}$$

where $\mu(k, a)$ and $\gamma(k, a)$ are two scale and time dependent functions introduced to incorporate any modified theory of gravity. Note the appearance of Ψ instead of Φ in the first equation. In the quasi-static approximation $\mu(k, a)$ and $\gamma(k, a)$ can be expressed as [43]

$$\mu(k, a) = A^2(\phi)(1 + \varepsilon(k, a)), \tag{20}$$

$$\gamma(k, a) = \frac{1 - \varepsilon(k, a)}{1 + \varepsilon(k, a)}, \tag{21}$$

where

$$\varepsilon(k, a) = \frac{2\beta^2(a)}{1 + m^2(a)\frac{a^2}{k^2}}. \tag{22}$$

Modification in the evolution of Ψ and Φ in turn modifies the evolution of matter perturbation to as

$$\delta'' + \mathcal{H}\delta' - \frac{3}{2}\Omega_m \mathcal{H}^2 \mu(k, a)\delta = 0 \tag{23}$$

where $\mathcal{H} = a'/a$.

3 Dynamical dark energy model

The current measurements of cosmic expansion [55–57], indicate that the present Universe is dominated by dark energy (DE). The most common dark energy candidate is cosmological constant Λ representing a constant energy density occupying the space homogeneously. The equation of state parameter for DE in cosmological constant model is $w_{DE} = \frac{P_{DE}}{\rho_{DE}} = -1$. However a constant Λ makes the near coincidence of Ω_Λ and Ω_m in the present epoch hard to explain naturally. This gives way for other models of DE such as quintessence [58–60], interacting dark energy [61] and phenomenological parametrization of DE such as DDE [62–66]. In the phenomenological DE models the equation

of state parameter is taken to be a variable, dependent on the scale factor (equivalently redshift), i.e.,

$$w(z) = \sum_n w_n x(z), \tag{24}$$

where w_n are parameters fixed by observations and $x(z)$ is function of redshift. The most commonly followed $w(z)$ dependence are phantom fields ($w(z) < -1$) and non phantom field ($-1 \leq w(z) \leq 1$). In this paper we use the Chavallier–Polarski–Linder (CPL) [62,63] parametrization of DDE. The equation of state parameter for DE in CPL parametrization is

$$w_{DE}(z) = w_0 + w_a \frac{z}{z+1}, \tag{25}$$

where w_0 and w_a are the CPL parameters. This parametrization describes a non phantom field when $w_a + w_0 \geq -1$ and $w_0 \geq -1$. Choosing $w_0 = -1$ and $w_a = 0$ Eq. 25 gives back the Λ CDM model. As a result of this parametrization the evolution of DE density fraction is given by the equation

$$\Omega_{DE}(z) = \Omega_{DE,0}(1+z)^{3(1+w_0+w_a)} e^{-3w_a \frac{z}{z+1}}, \tag{26}$$

where $\Omega_{DE,0}$ is the DE density at present.

4 Massive neutrino in cosmology

Neutrinos play an important role in the evolution of the Universe. Several neutrino oscillation experiments have established that neutrinos are massive [67,68]. Massive neutrinos can affect the background as well as matter perturbation which in turn can leave its imprint on cosmological observations. In the early universe, neutrinos are relativistic and interact weakly with other particles. As the temperature of the Universe decreases, the weak interaction rate becomes less than the Hubble expansion rate of the Universe and neutrinos decouple from rest of the plasma. Since neutrinos are relativistic, their energy density after decoupling is given [69,70]

$$\rho_\nu = \left[\frac{7}{8} \left(\frac{4}{11} \right)^{4/3} N_{\text{eff}} \right] \rho_\gamma, \tag{27}$$

where ρ_γ is the photon energy density. N_{eff} is the effective number of relativistic neutrinos at early times which is theoretically predicted to be 3.045 [71] and estimated from CMB observation to be 2.99 ± 0.17 [72]. When the temperature of the Universe goes below the mass of the neutrinos, they turn into non-relativistic particles. The energy density fraction of neutrinos in the present universe depends on the sum of their masses and is given as

$$\Omega_\nu = \frac{\sum m_\nu}{\text{eV}} \frac{1}{93.1 h^2}, \tag{28}$$

where $\sum m_\nu$ is the sum of neutrino masses. Neutrinos in the present Universe contribute a very small fraction of energy density however they can affect the formation of structure at large scales.

After neutrinos decouple, they behave as collisionless fluid with individual particles streaming freely. The free streaming length is equal to the Hubble radius for the relativistic neutrinos, whereas non-relativistic neutrinos stream freely on the scales $k > k_{\text{fs}}$, where k_{fs} is the neutrino free-streaming scale. On the scales $k > k_{\text{fs}}$, the free-streaming of the neutrinos damp the neutrino density fluctuations and suppress the power in the matter power spectrum. On the other hand neutrinos behave like cold dark matter perturbations on the scales $k < k_{\text{fs}}$ [69,70].

4.1 Evolution equations for massive neutrinos

Massive neutrinos obey the collisionless Boltzmann equation, therefore we solve the Boltzmann equation for the neutrinos to get their evolution equations. The energy momentum tensor for neutrinos is given as

$$T_{\mu\nu} = \int dP_1 dP_2 dP_3 (-g)^{-1/2} \frac{P_\mu P_\nu}{p^0} f(x^i, P_j, \tau), \tag{29}$$

where $f(x^i, P_j, \tau)$ and P_μ are the distribution function and the four momentum of neutrinos respectively. We expand the distribution function around the zeroth-order distribution function f_0 as

$$f(x^i, P_j, \tau) = f_0(q)[1 + \chi(x^i, P_j, \tau)], \tag{30}$$

where χ is the perturbation in the distribution function. Using Eqs. 29 in 30 and equating the zeroth order terms, we get the unperturbed energy density and pressure for neutrinos

$$\bar{\rho} = 4\pi a^{-4} \int q^2 dq \varepsilon f_0(q), \quad \bar{P} = \frac{4\pi a^{-4}}{3} \int q^2 dq \frac{q^2}{\varepsilon} f_0(q). \tag{31}$$

Similarly, We get the perturbed quantities by equating the first order terms

$$\begin{aligned} \delta\rho &= 4\pi a^{-4} \int q^2 dq \varepsilon f_0(q) \chi, \\ \delta P &= \frac{4\pi a^{-4}}{3} \int q^2 dq \frac{q^2}{\varepsilon} f_0(q) \chi, \\ \delta T_i^0 &= 4\pi a^{-4} \int q^2 dq q n_i f_0(q) \chi, \\ \delta \Sigma_j^i &= \frac{4\pi a^{-4}}{3} \int q^2 dq \frac{q^2}{\varepsilon} \left(n_i n_j - \frac{1}{3} \delta_{ij} \right) f_0(q) \chi, \end{aligned} \tag{32}$$

where $q_i = qn_i$ is the co-moving momentum and $\varepsilon = \varepsilon(q, \tau) = \sqrt{q^2 + m_\nu^2 a^2}$. It is clear from eq. 32 that we can not simply integrate out the q dependence as ε is the function of both τ and q . Hence, we will use the Legendre series expansion of the perturbation χ to get the perturbed evolution equations for the massive neutrino. Legendre series expansion of the perturbation χ is given as

$$\chi(\mathbf{k}, \hat{n}, q, \tau) = \sum_{l=0}^{\infty} (-i)^l (2l + 1) \chi_l(\mathbf{k}, q, \tau) P_l(\hat{k} \cdot \hat{n}). \quad (33)$$

Using Eq. 33 in the Eq. 32, we get the perturbed evolution equations for the massive neutrino [73]

$$\begin{aligned} \delta\rho_h &= 4\pi a^{-4} \int q^2 dq \varepsilon f_0(q) \chi_0, \\ \delta P_h &= \frac{4\pi}{3} a^{-4} \int q^2 dq \frac{q^2}{\varepsilon} f_0(q) \chi_0, \\ (\bar{\rho}_h + \bar{P}_h)\theta_h &= 4\pi k a^{-4} \int q^2 dq q f_0(q) \chi_1, \\ (\bar{\rho}_h + \bar{P}_h)\sigma_h &= \frac{8\pi}{3} a^{-4} \int q^2 dq \frac{q^2}{\varepsilon} f_0(q) \chi_2, \end{aligned} \quad (34)$$

where the Boltzmann equation governs the evolution of χ_l . In the Newtonian gauge Boltzmann equations for χ_l are given as

$$\begin{aligned} \dot{\chi}_0 &= -\frac{qk}{\varepsilon} \chi_1 - \dot{\Phi} \frac{d \ln f_0}{d \ln q}, \\ \dot{\chi}_1 &= \frac{qk}{3\varepsilon} (\chi_0 - 2\chi_2) - \frac{\varepsilon k}{3q} \Psi \frac{d \ln f_0}{d \ln q}, \\ \dot{\chi}_l &= \frac{qk}{(2l + 1)\varepsilon} [l\chi_{l-1} - (l + 1)\chi_{l+1}], \quad \text{for } l \geq 2. \end{aligned} \quad (35)$$

5 Matter power spectrum and σ_8

In this section we discuss the effect of massive neutrinos, HS model parameters and DDE model parameters on the matter power spectrum and σ_8 . Matter power spectrum is a scale dependent quantity defined as the two-point correlation function of matter density, $P(k) = k^{n_s} T^2(k) D^2(a)$. Where $T(k)$ is the matter transfer function, $D(a)$ is the linear growth factor and n_s is the tilt of the primordial power spectrum. Also, the r.m.s. fluctuation of density perturbations in a sphere of radius r is defined as

$$\sigma(r, z) = \left[\frac{1}{2\pi^2} \int_0^\infty dk k^2 P(k, z) |W(kr)|^2 \right]^{1/2}, \quad (36)$$

where r is related to mass by $r = (3M/4\pi\rho_m(z = 0))^{1/3}$ with $\rho_m(z = 0)$ being the matter density of the Universe at present epoch. Here $W(kr) = 3(\sin kr - kr \cos kr)/(kr)^3$ is the filter function. This is a scale dependent quantity. The

r.m.s. fluctuation of density perturbations on scale $8 h^{-1} \text{Mpc}$ is called $\sigma_8(z)$.

We use CAMB [74] to generate the matter power spectrum for DDE model, whereas we use MGCAMB [50, 51] to obtain the matter power spectrum for HS model. In order to see the effect of modified gravity models and massive neutrinos we plot matter power spectrum for some bench mark values of $\sum m_\nu$, HS model parameters and DDE model parameters. The power spectra are shown in Fig. 1.

- As we discussed in Sect. 4, massive neutrinos stream freely on the scales $k > k_{fs}$ and they can escape out of the high density regions on those scales. The perturbations on length scales smaller than neutrino free streaming length will be washed out and therefore power spectrum gets suppress on these scales. Neutrino mass cuts the power at length scales even larger than the $8 h^{-1} \text{Mpc}$ which requires a large Ω_m which in turn disfavors the compatibility of $\sigma_8 - \Omega_m$ between the two observations.

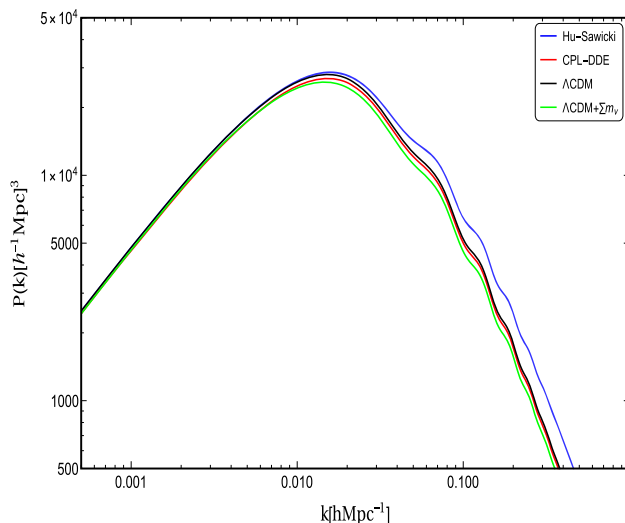


Fig. 1 Matter power spectrum in HS, DDE and Λ CDM model

Table 1 Parameters with flat priors are listed in this table

Parameters	Planck + BAO	LSS
$\Omega_c h^2$	[0.001, 0.99]	[0.001, 0.99]
$\Omega_b h^2$	[0.005, 0.1]	[0.005, 0.1]
τ_{reio}	[0.01, 0.8]	
$100\theta_{MC}$	[0.5, 10]	[0.5, 10]
$\ln(10^{10} A_s)$	[2, 4]	[2, 4]
n_s	[0.8, 1.2]	[0.8, 1.2]
$\sum M_\nu$	[0, 5.0]	[0, 5.0]
$\log_{10} f_{R_0}$	[-9.0, 10]	[-9.0, 10]

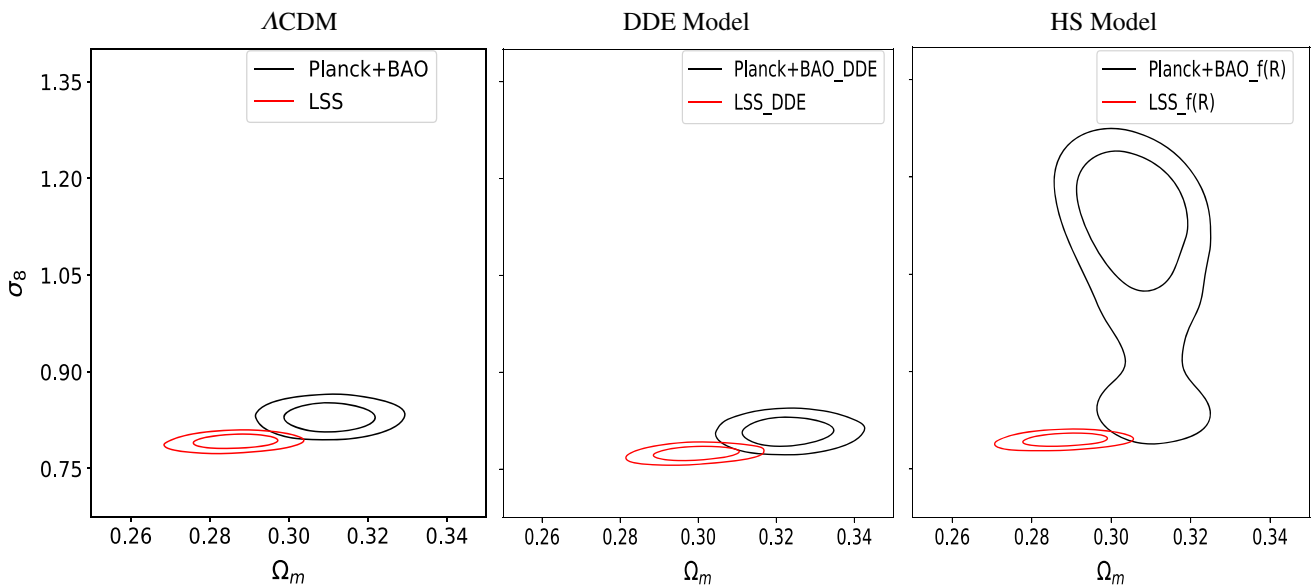


Fig. 2 The 1- σ and 2- σ contours in $\sigma_8 - \Omega_m$ parameter space for Λ CDM, DDE and HS model with $\sum m_\nu = 0.06$ eV are shown here. It is shown that the σ_8 discrepancy worsens in the HS model whereas in DDE model the discrepancy is somewhat relieved

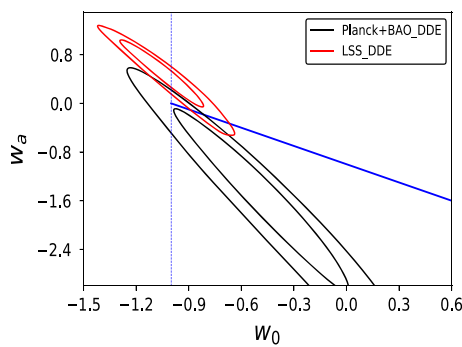


Fig. 3 Parameter space for w_0 and w_a allowed by Planck + BAO and LSS data. Blue and Blue dashed lines correspond to $w_0 + w_a = -1$ and $w_0 = -1$ respectively. The region above these lines is the non-phantom region

- DDE cuts the power spectrum at all length scales. Since, in the DDE model, dark energy density increases with the redshift, therefore, in the early time when the dark energy density is large, the power cut is more prominent at small scales.
- On the other hand, the power spectrum gets affected in an opposite manner for HS model as the power increases slightly on small length scales.

6 Datasets and analysis

As discussed in Sect. 1 there is a discrepancy in the values of H_0 and σ_8 reported by the large scale surveys and Planck CMB observations. In this paper we analyse Λ CDM, HS

Table 2 The best fit values with 1- σ error for all the parameters with fixed $\sum m_\nu$, obtained from the MCMC analyses for all the models considered are listed here

Parameter	Λ CDM		DDE		HS	
	Planck + BAO	LSS	Planck + BAO	LSS	Planck + BAO	LSS
$\Omega_b h^2$	0.02227 ± 0.00020	0.02274 ± 0.00081	0.02236 ± 0.00020	0.02292 ± 0.00080	0.02243 ± 0.00022	0.02225 ± 0.00070
$\Omega_c h^2$	0.1190 ± 0.0013	0.1159 ± 0.0016	0.1178 ± 0.0013	0.1146 ± 0.0016	0.1185 ± 0.0013	0.1153 ± 0.0015
$100\theta_{MC}$	1.04098 ± 0.00042	1.0425 ± 0.0011	1.04116 ± 0.00042	1.0427 ± 0.0011	1.04108 ± 0.00043	1.0419 ± 0.0010
τ_{reio}	0.081 ± 0.018	0.08	0.086 ± 0.018	0.086	0.063 ± 0.020	0.65
$\ln(10^{10} A_s)$	3.094 ± 0.035	3.080 ± 0.012	3.101 ± 0.036	3.095 ± 0.011	3.058 ± 0.041	3.053 ± 0.011
n_s	0.9673 ± 0.0044	0.905 ± 0.019	0.9701 ± 0.0045	0.910 ± 0.019	0.9691 ± 0.0047	0.941 ± 0.011
H_0	67.65 ± 0.57	$69.81^{+0.73}_{-0.82}$	66.02 ± 0.52	67.98 ± 0.72	68.00 ± 0.61	69.26 ± 0.72
Ω_m	0.3102 ± 0.0077	0.2862 ± 0.0071	0.3230 ± 0.0077	0.2991 ± 0.0073	0.3062 ± 0.0079	0.2882 ± 0.0071
σ_8	0.829 ± 0.015	0.7917 ± 0.0074	0.808 ± 0.015	0.7745 ± 0.0074	$1.10^{+0.12}_{-0.030}$	0.7948 ± 0.0068
S_8	0.840 ± 0.018	$0.7732^{+0.0139}_{-0.0119}$	0.834 ± 0.018	$0.7732^{+0.0141}_{-0.0122}$	$1.105^{+0.110}_{-0.020}$	$0.7790^{+0.0137}_{-0.0119}$

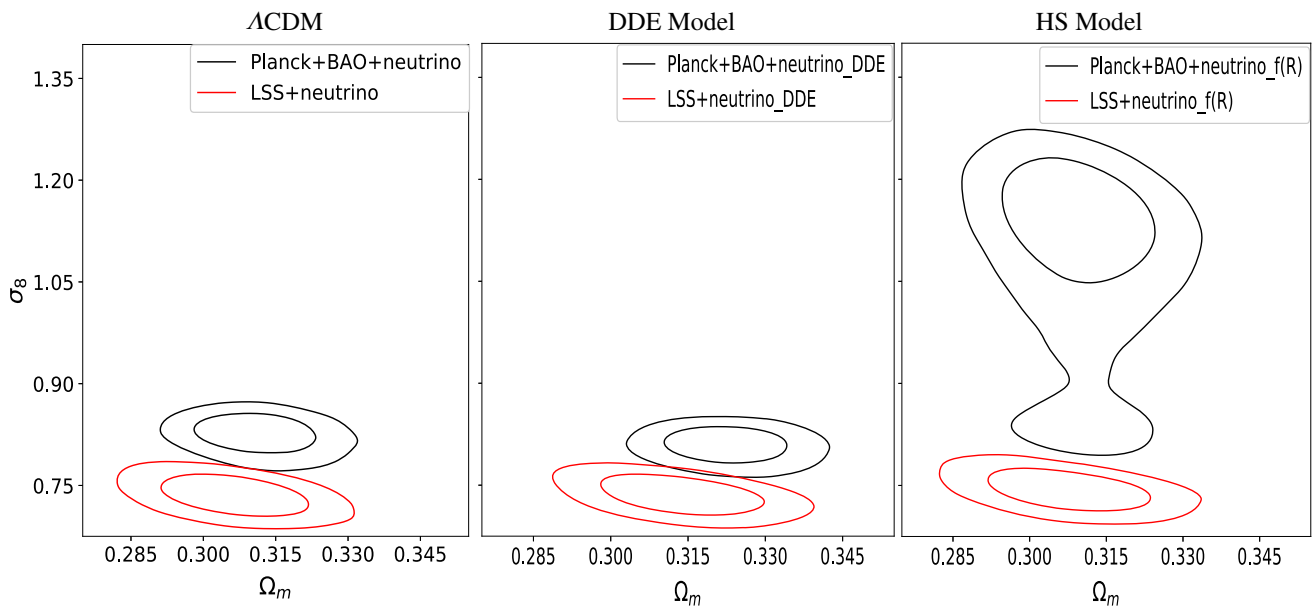


Fig. 4 The 1- σ and 2- σ contours in $\sigma_8 - \Omega_m$ parameter space for Λ CDM, DDE and HS model with varying Σm_ν are shown here. It is shown that the σ_8 discrepancy worsens in the HS model whereas in DDE model the discrepancy is somewhat relieved

Table 3 The best fit values with 1- σ error for all the parameters with varying Σm_ν , obtained from the MCMC analyses for all the models considered are listed here

Parameter	Λ CDM		DDE		HS	
	Planck + BAO	LSS	Planck + BAO	LSS	Planck + BAO	LSS
$\Omega_b h^2$	0.02228 ± 0.00020	0.02277 ± 0.00080	0.02236 ± 0.00020	0.02283 ± 0.00081	0.02254 ± 0.00025	$0.02216^{+0.00064}_{-0.00073}$
$\Omega_c h^2$	$0.1188^{+0.0015}_{-0.0014}$	0.1141 ± 0.0018	0.1177 ± 0.0014	0.1134 ± 0.0017	$0.1172^{+0.0020}_{-0.0017}$	0.1139 ± 0.0017
$100\theta_{MC}$	1.04097 ± 0.00042	1.0430 ± 0.0011	1.04114 ± 0.00042	1.0431 ± 0.0011	1.04120 ± 0.00045	1.0434 ± 0.0010
τ_{reio}	$0.082^{+0.018}_{-0.020}$	0.082	0.086 ± 0.018	0.086	0.065 ± 0.021	0.065
$\ln(10^{10} A_s)$	3.096 ± 0.037	3.114 ± 0.015	3.101 ± 0.036	3.117 ± 0.015	3.058 ± 0.042	3.085 ± 0.014
n_s	$0.9676^{+0.0045}_{-0.0050}$	0.911 ± 0.019	0.9702 ± 0.0047	0.913 ± 0.019	$0.9723^{+0.0053}_{-0.0060}$	0.943 ± 0.011
H_0	67.56 ± 0.65	67.80 ± 0.99	66.05 ± 0.57	66.65 ± 0.97	67.64 ± 0.74	67.45 ± 0.96
Ω_m	0.3112 ± 0.0082	0.306 ± 0.010	0.3227 ± 0.0079	0.314 ± 0.011	0.3096 ± 0.0089	0.307 ± 0.010
σ_8	$0.826^{+0.022}_{-0.017}$	0.735 ± 0.028	$0.809^{+0.019}_{-0.016}$	0.735 ± 0.020	$1.115^{+0.091}_{-0.034}$	0.743 ± 0.020
Σm_ν	< 0.157	0.364 ± 0.095	< 0.116	0.275 ± 0.095	< 0.318	0.333 ± 0.093
S_8	0.838 ± 0.022	$0.7431^{+0.0201}_{-0.0181}$	0.835 ± 0.020	$0.7522^{+0.0201}_{-0.0172}$	$1.127^{+0.089}_{-0.031}$	$0.7522^{+0.0201}_{-0.0175}$

and DDE model. For analyzing these models, we use Planck CMB observations [1] for temperature anisotropy power spectrum over the multipole range $\ell \sim 2 - 2500$ and Planck CMB polarization data for low ℓ only. We refer to these data sets combined as Planck data. We also use the baryon acoustic oscillations(BAO) data from 6dF Galaxy Survey [75], BOSS DR11 [76, 77] and SDSS DR7 Main Galaxy Sample [78]. In addition we use the cluster count data from Planck SZ survey [79], lensing data from Canada France Hawaii Telescope Lensing Survey (CFHTLens) [80, 81] and CMB lensing data from Planck lensing survey [82] and South Pole Telescope (SPT) [83, 84]. We also use the data for Redshift space dis-

tortions (RSD) from BOSS DR11 RSD measurements [85]. We combine Planck SZ data, CFHTLens data, Planck lensing data, SPT lensing data and RSD data and refer them as LSS data. We perform Markov Chain Monte Carlo(MCMC) analysis for Λ CDM, HS and DDE model with both Planck + BAO and LSS data. We use CosmoMC [86] to perform the MCMC analysis for Λ CDM and DDE model and add MGCosmoMC patch [50, 51] to it for HS model. MGCosmoMC patch includes the $\mu(k, a)$ and $\gamma(k, a)$ parametrization discussed in Sect. 2.

In our analysis for Λ CDM model we have total six free parameter which are standard cosmological parameters

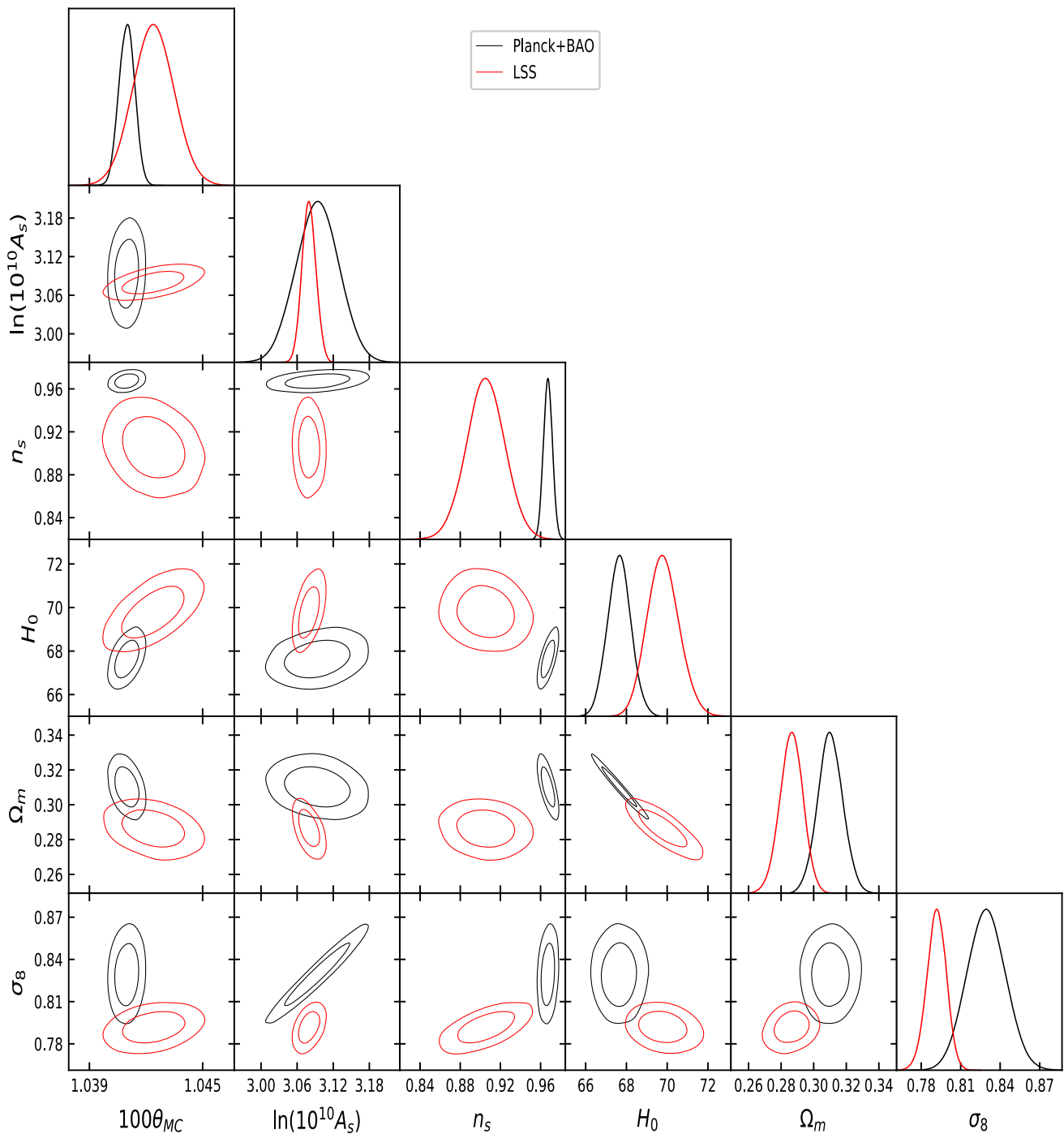


Fig. 5 The triangle plot showing 1- σ and 2- σ contours of all the parameters for Λ CDM model with $\sum m_\nu = 0.06\text{eV}$ is shown here

namely, density parameters for cold dark matter(CDM) Ω_c and baryonic matter Ω_b , optical depth to re-ionization τ_{reio} , angular acoustic scale θ_{MC} , amplitude A_s and tilt n_s of the primordial power spectrum. We fix $\sum m_\nu = 0.06\text{eV}$ to satisfy the neutrino oscillation experiments results. We also have two derived parameters H_0 and σ_8 . First we perform MCMC analysis with Planck + BAO data with these parameters and

get constraints for each parameter. Next, we run the MCMC analysis with LSS data for Λ CDM model. Since τ_{reio} does not affects the LSS observation therefore we also use the best fit value of $\tau_{reio} = 0.08$, obtained from analysis with Planck + BAO data, as fixed prior. We have listed all the parameters with flat in Table 1. These analyses give $\sigma_8 = 0.829 \pm 0.015$ for the Planck + BAO data and $\sigma_8 = 0.7917 \pm 0.0074$ and

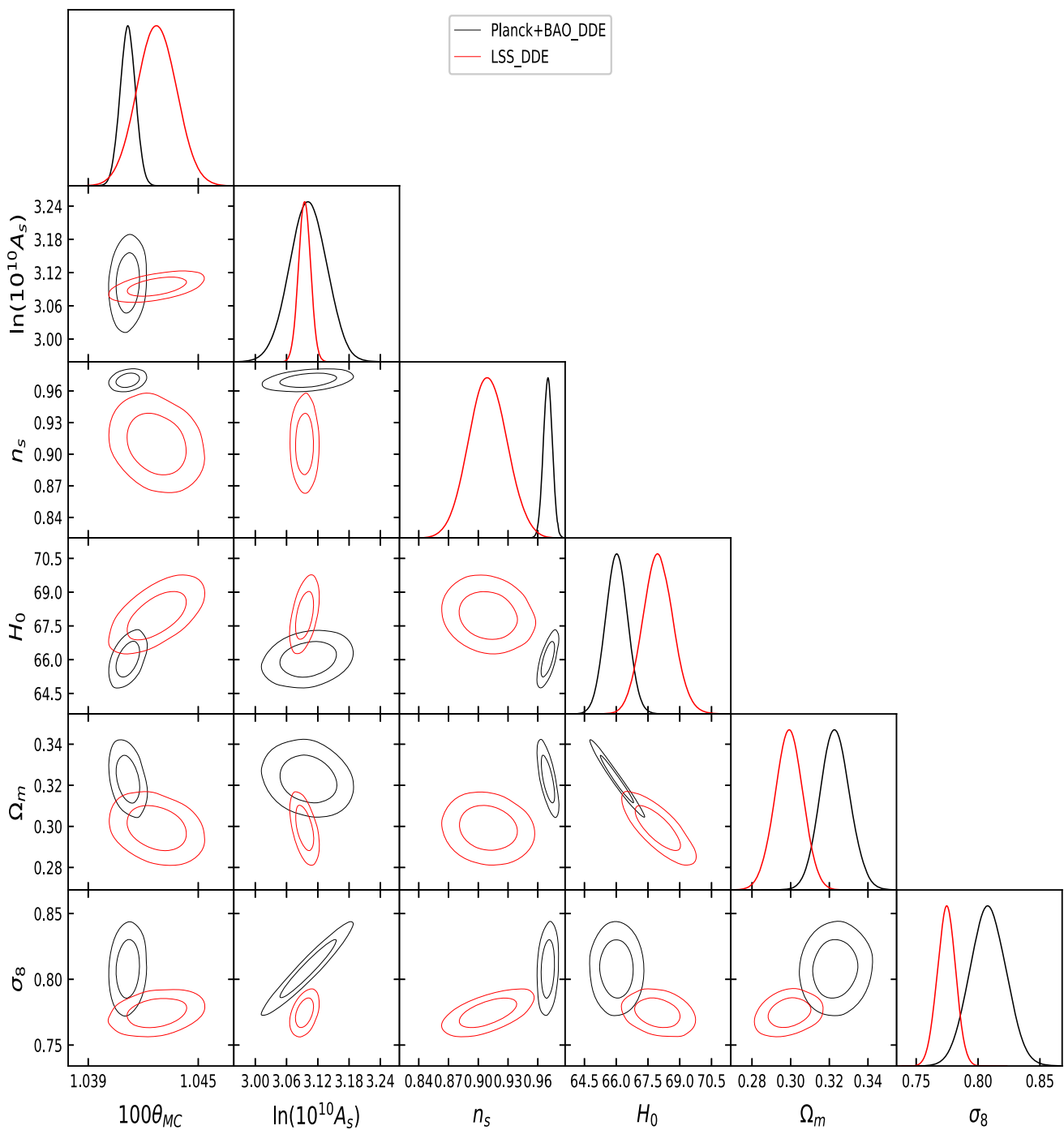


Fig. 6 The triangle plot showing 1- σ and 2- σ contours of all the parameters for DDE model with $\sum m_\nu = 0.06$ eV is shown here

for LSS data. We plot the parameter space $\sigma_8 - \Omega_m$, obtained from two different analysis (Fig. 2). It is clear from the Fig. 2 that there is a mismatch between the values of σ_8 inferred from Planck + BAO data and that from LSS data.

In our analysis for HS model we have total eight free parameter of which six are standard cosmological parameters, two are HS model parameters namely, f_{R0} and n as defined in Sect. 2. Here we fix $n = 1$ and allowed f_{R0} to

vary in the range $[10^{-9}, 10]$. We repeat the whole procedure to do the analysis with Planck + BAO and LSS data for HS model and obtain constraints for each parameter. Similar to the analysis for Λ CDM model, in the analysis of this model with LSS data, we fixed the $\tau_{reio} = 0.065$. The best fit values for σ_8 in this analysis are $1.10^{+0.12}_{-0.030}$ with Planck + BAO data and 0.7948 ± 0.0068 with LSS data. We plot the parameter space $\sigma_8 - \Omega_m$, obtained from analysis with two different

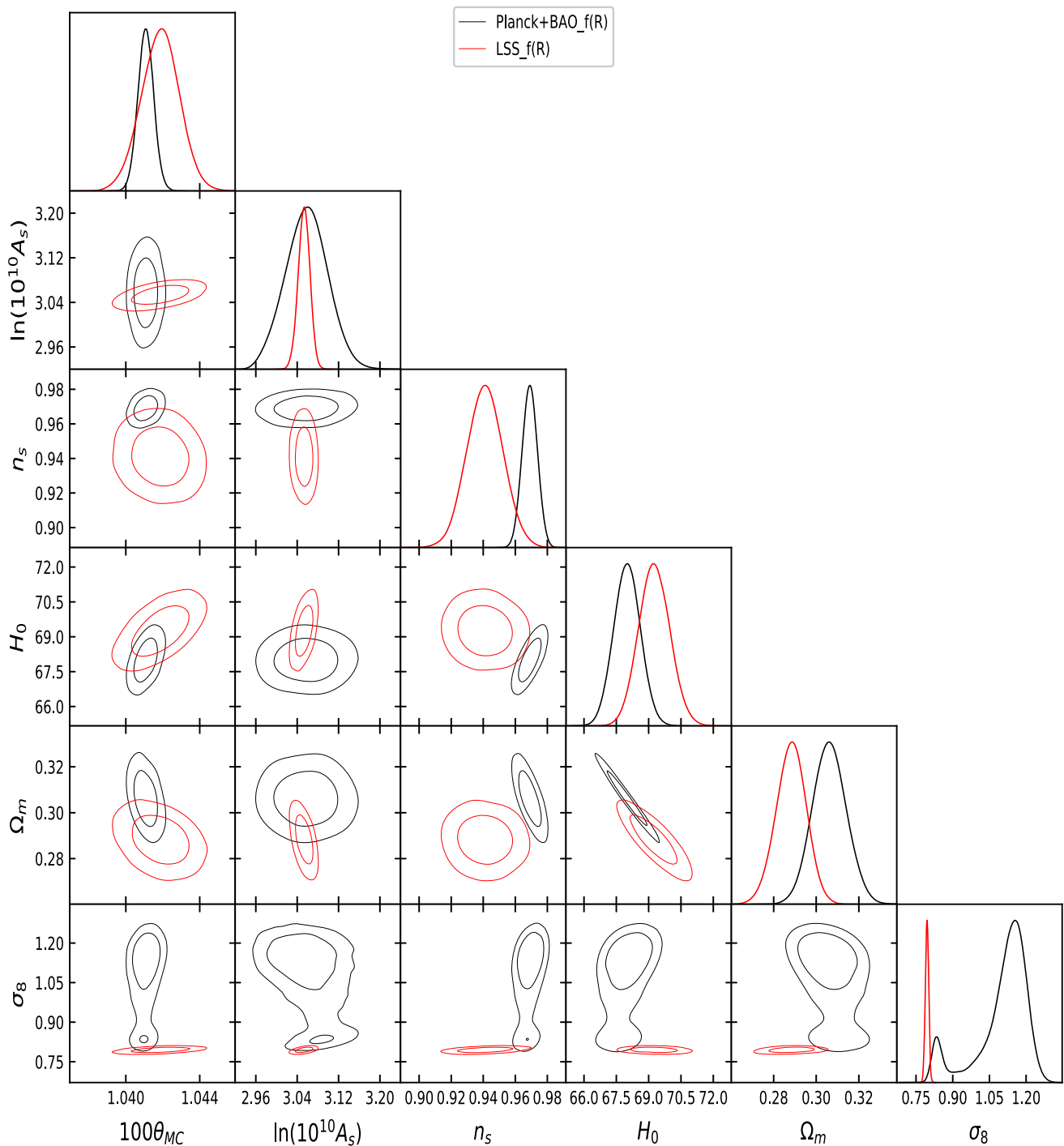


Fig. 7 The triangle plot showing 1- σ and 2- σ contours of all the parameters for HS model with $\sum m_\nu = 0.06$ eV is shown here

data sets, see Fig. 2. We found that tension between the values of σ_8 inferred from Planck + BAO data and that from LSS data is increases.

Next we do the analysis for DDE model. In our analysis for DDE model, in addition to the six standard parameters, we have two model parameters w_0 and w_a as defined in Sect. 3 making a total of eight parameters. First we do the MCMC

analysis for both the data sets keeping w_a and w_0 as free parameters and get the 2- σ allowed ranges which are shown in Fig. 3. Next we put the non-phantom constraints represented by region above blue and dashed blue lines in Fig. 3. We see that the region allowed by both the data sets and also satisfies the non phantom conditions $w_a + w_0 \geq -1$ and $w_0 \geq -1$ is very small and close to $w_0 = -0.9$ and

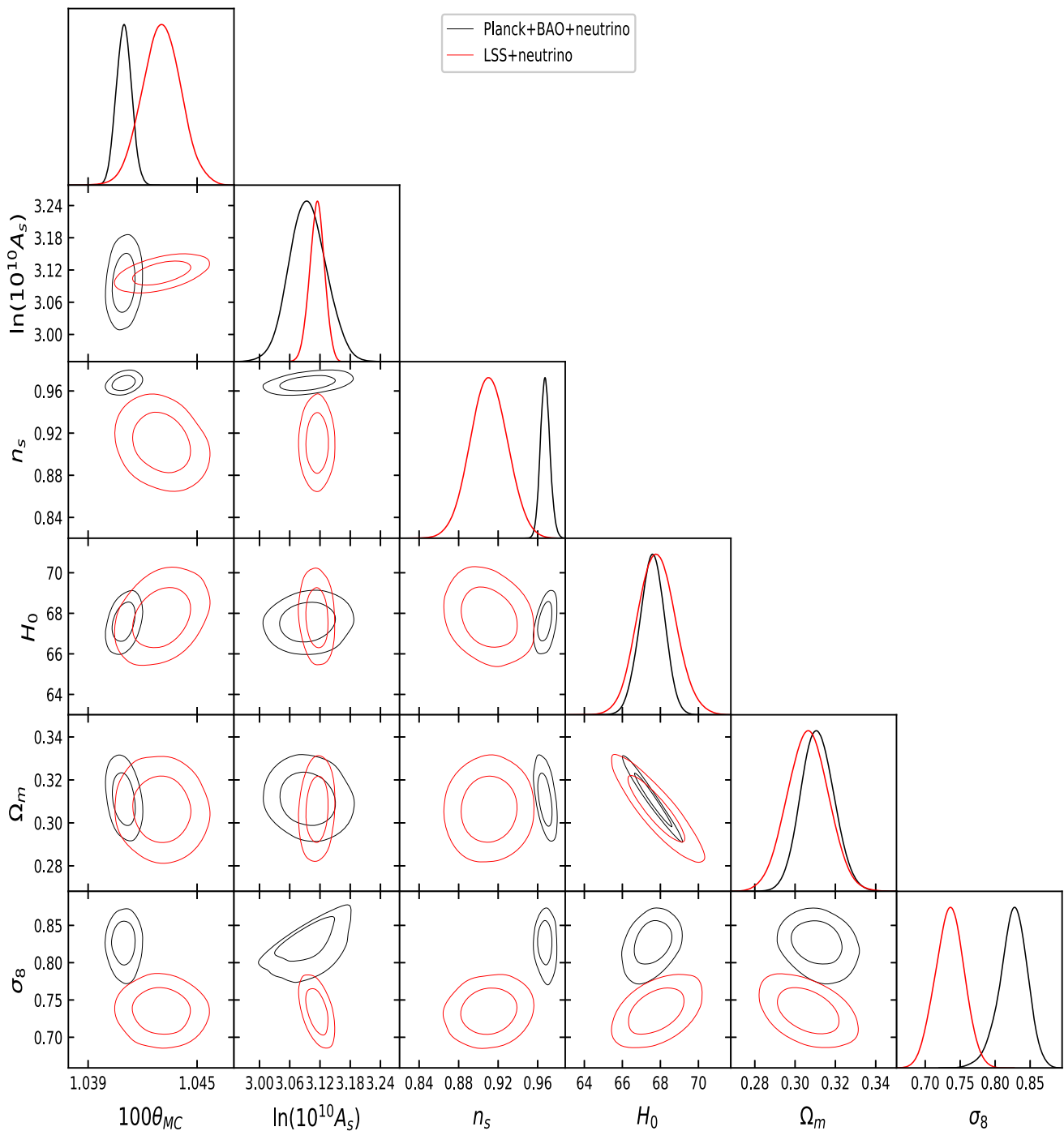


Fig. 8 The triangle plot showing 1- σ and 2- σ contours of all the parameters for Λ CDM model with $\sum m_\nu$ as free parameter is shown here

$w_a = -0.1$. Therefore we choose these values for our further analysis, and do MCMC analysis scan over the remaining six parameters. We repeat the same procedure as we did for Λ CDM and HS model. First we do analysis with Planck + BAO data and get constraints on all the free parameters. In the analysis with LSS data, we fix $\tau_{reio} = 0.086$ (This value is obtained in the analysis with Planck + BAO data). We plot the parameter space $\sigma_8 - \Omega_m$, obtained from analysis

with two different data sets, see Fig. 2. We find that tension between the values of σ_8 values inferred from Planck + BAO data and that from LSS data is somewhat alleviated in the DDE model. Constraints on σ_8 , H_0 , and other parameters for each model are listed in Table 2.

Next, we use sum of massive neutrino $\sum m_\nu$ as a free parameter and allow it to vary in the range $[0, 5]$ eV in our analysis for all three models. We repeat the whole procedure

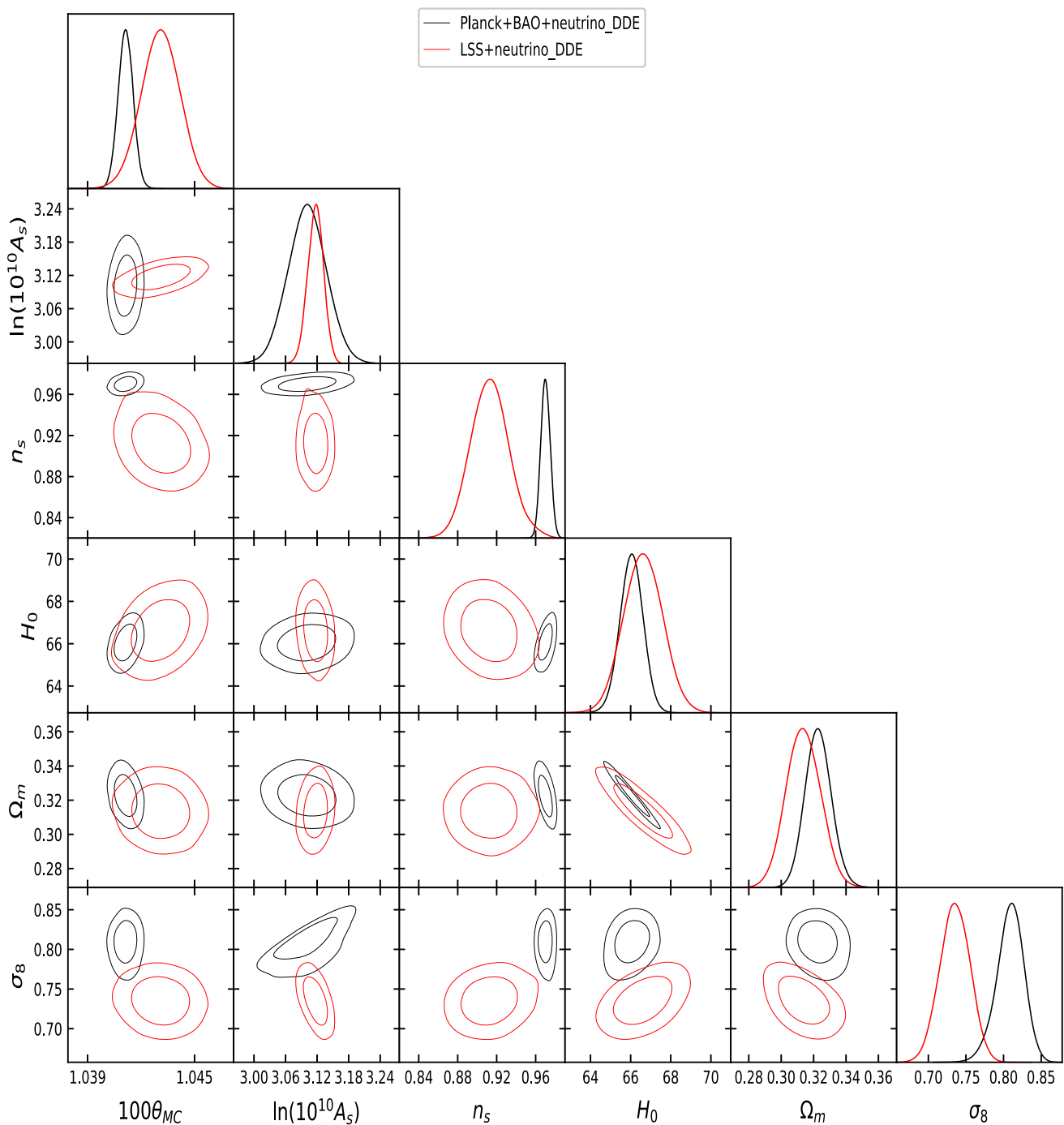


Fig. 9 The triangle plot showing 1- σ and 2- σ contours of all the parameters for DDE model with $\sum m_\nu$ as free parameter is shown here

and obtain constraints for each parameter. We plot the parameter space $\sigma_8 - \Omega_m$ for each model, see Fig. 4. Constraints on $\sum M_\nu$, σ_8 , H_0 and other parameters for each model are listed in Table 3. The triangle plots for all the three models with $\sum m_\nu = 0.06\text{eV}$ are shown Figs. 5, 6 and 7. The triangle plots for all the three models with $\sum m_\nu$ as free parameter are shown Figs. 8, 9 and 10. The corresponding 1 σ and 2 σ contours for $\sum M_\nu$ are shown in Fig. 11.

7 Discussion and conclusion

Galaxy surveys and CMB lensing measure the parameter $\sigma_8 \Omega_m^\alpha$, where Ω_m^α represents a model dependent growth function. In ΛCDM $\alpha = 0.5$ but it could be different for other DM-DE models. In CMB measurement of temperature anisotropy spectrum C_l and BAO determine Ω_m . The discrepancy between the CMB and LSS measurement is deter-

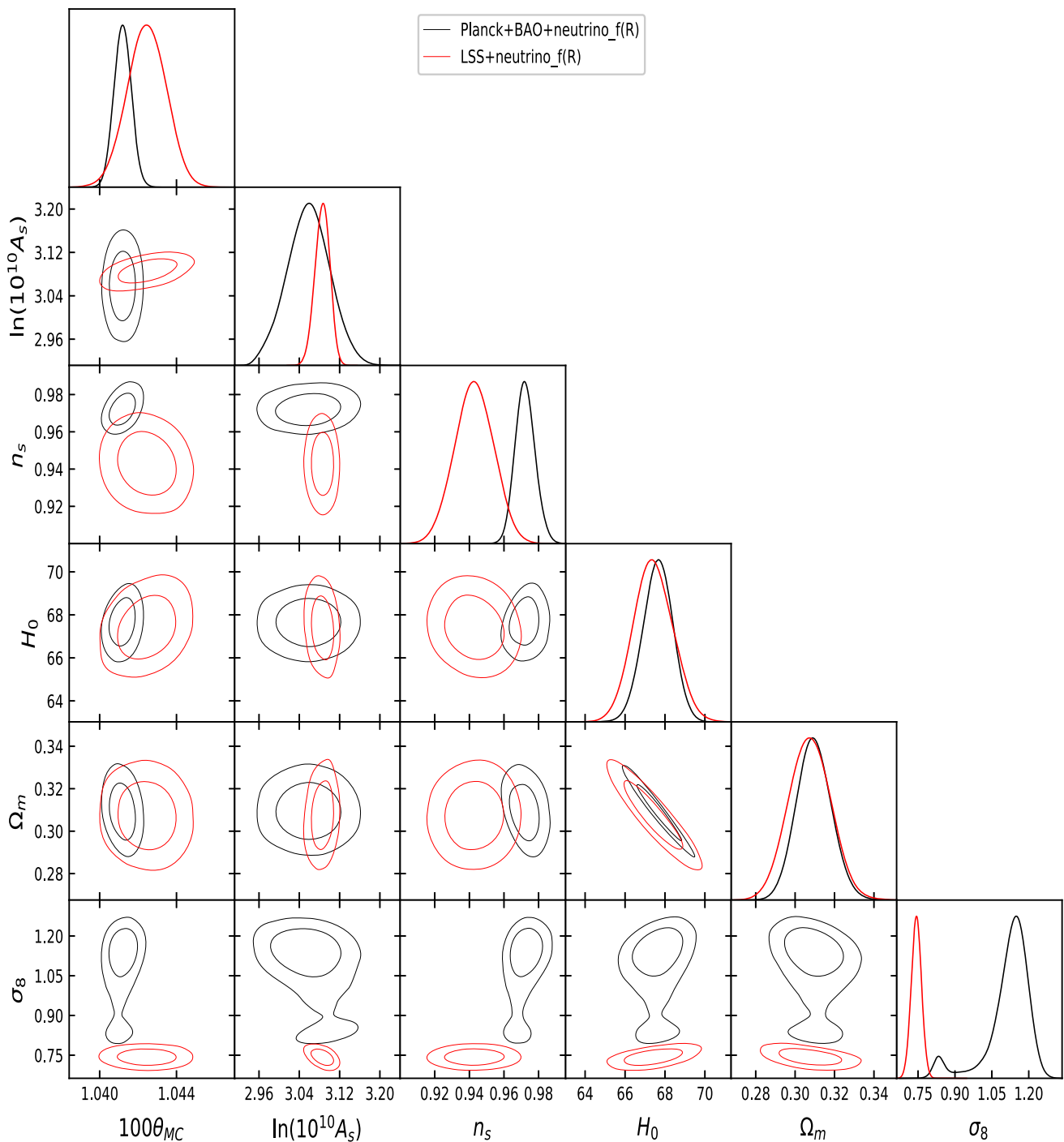


Fig. 10 The triangle plot showing 1- σ and 2- σ contours of all the parameters for HS model with $\sum m_\nu$ as free parameter is shown here

mined by the model dependent growth function Ω_m^α . The growth function can thus be used for testing theories of gravity and dynamical DE. In the present paper we tested HS and DDE models in the context of $\sigma_8 - \Omega_m$ observations. We find that in the HS model the $\sigma_8 - \Omega_m$ tension worsens compared to the Λ CDM model. On the other hand in the DDE model there is slight improvement in the concordance

between the two data sets. The discrepancy levels between values inferred from Planck + BAO and LSS data for Λ CDM, DDE and HS model are listed in Table 4. We also find that adding active massive neutrinos allow us to have larger value of Ω_m . $H(z)$ in $H(z) = H_0\sqrt{\Omega_m(1+z)^3 + \Omega_\Lambda}$ is determined by the observation, therefore a larger value of Ω_m brings down the H_0 value to satisfy the observation. Thus,

Fig. 11 Bounds on the Neutrino mass in DDE, HS and Λ CDM models with Planck and LSS data

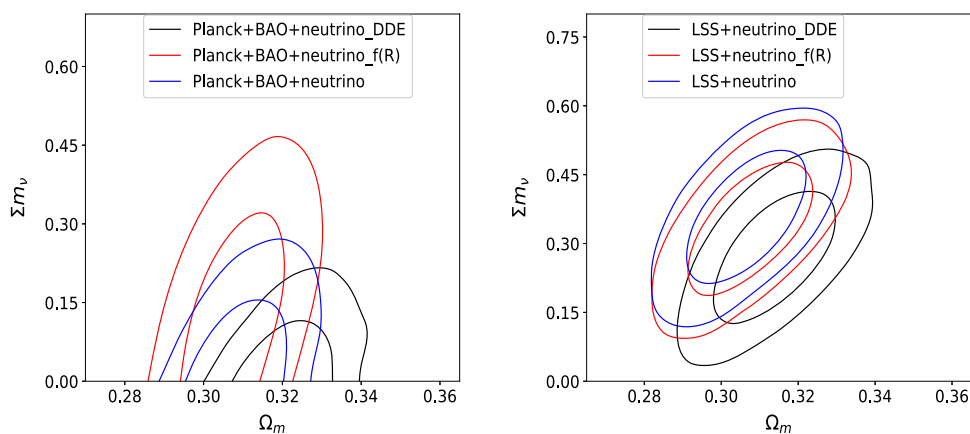


Table 4 The discrepancy level between the σ_8 values inferred from Planck + BAO and LSS data for Λ CDM, DDE and HS model are listed here

	Λ CDM	DDE	HS
With fixed $\sum M_\nu$	1.722σ	1.522σ	1.793σ
With varying $\sum M_\nu$	1.960σ	1.796σ	2.273σ

we find that the H_0 tension between CMB and LSS observations is resolved by using active massive neutrinos. However, this increases the mismatch between H_0 values obtained from LSS and SN-Ia observations. In all three models, the n_s values obtained in the analysis with LSS data is smaller as compared to n_s value obtained from Planck + BAO. Which gives rise to another tension between the two data sets. The tilt of the primordial spectrum is calculated at a particular pivot scale (k_*). In our analysis the pivot scale is 0.05 Mpc^{-1} . The n_s discrepancy may be due to the fact that Planck data and LSS data have different pivot scale which can be a signature of running tilt of the primordial spectrum. This can be checked in future works. The bounds on neutrino mass become more stringent in the DDE model. In the HS model there is a loosening in the analysis with Planck data and not much effect in the analysis with the LSS data. In conclusion we see that σ_8 measurement from CMB and LSS experiments can be used as a probe of modified gravity or quintessence models. Future observations of CMB and LSS may shrink the parameter space for $\sigma_8 - \Omega_m$ and then help in selecting the correct $f(R)$ and DDE theory.

Acknowledgements We thank the anonymous referee for many useful insights and suggestions which helped in improving the overall quality of the work. We also acknowledge the computation facility, 100TFLOP HPC Cluster, Vikram-100, at Physical Research Laboratory, Ahmedabad, India.

Data Availability Statement This manuscript has associated data in a data repository. [Authors' comment: The data sets used in this work are available in the repository of the publicly available code CosmoMC. <https://doi.org/10.1103/PhysRevD.66.103511>.]

Open Access This article is distributed under the terms of the Creative Commons Attribution 4.0 International License (<http://creativecommons.org/licenses/by/4.0/>), which permits unrestricted use, distribution, and reproduction in any medium, provided you give appropriate credit to the original author(s) and the source, provide a link to the Creative Commons license, and indicate if changes were made. Funded by SCOAP³.

References

1. P.A.R. Ade, Planck 2015 results. XIII. Cosmological parameters. *Astron. Astrophys.* **594**, A13 (2016)
2. A. Vikhlinin, Chandra cluster cosmology project III: cosmological parameter constraints. *Astrophys. J.* **692**, 1060–1074 (2009)
3. E. Macaulay, I.K. Wehus, H.K. Eriksen, Lower growth rate from recent redshift space distortion measurements than expected from planck. *Phys. Rev. Lett.* **111**(16), 161301 (2013)
4. R.A. Battye, T. Charnock, A. Moss, Tension between the power spectrum of density perturbations measured on large and small scales. *Phys. Rev. D* **91**(10), 103508 (2015)
5. N. MacCrann, J. Zuntz, S. Bridle, B. Jain, M.R. Becker, Cosmic discordance: are planck CMB and CFHTLenS weak lensing measurements out of tune? *Mon. Not. R. Astron. Soc.* **451**(3), 2877–2888 (2015)
6. K. Aylor et al., A comparison of cosmological parameters determined from CMB temperature power spectra from the south pole telescope and the planck satellite. *Astrophys. J.* **850**(1), 101 (2017)
7. M. Raveri, Are cosmological data sets consistent with each other within the Λ cold dark matter model? *Phys. Rev. D* **93**(4), 043522 (2016)
8. W. Lin, M. Ishak, Cosmological discordances: a new measure, marginalization effects, and application to geometry versus growth current data sets. *Phys. Rev. D* **96**(2), 023532 (2017)
9. A. Pourtsidou, T. Tram, Reconciling CMB and structure growth measurements with dark energy interactions. *Phys. Rev. D* **94**(4), 043518 (2016)
10. V. Salvatelli, N. Said, M. Bruni, A. Melchiorri, D. Wands, Indications of a late-time interaction in the dark sector. *Phys. Rev. Lett.* **113**(18), 181301 (2014)
11. W. Yang, X. Lixin, Cosmological constraints on interacting dark energy with redshift-space distortion after Planck data. *Phys. Rev. D* **89**(8), 083517 (2014)
12. P. Ko, Y. Tang, Light dark photon and fermionic dark radiation for the Hubble constant and the structure formation. *Phys. Lett. B* **762**, 462–466 (2016)
13. P. Ko, Y. Tang, Residual non-Abelian dark matter and dark radiation. *Phys. Lett. B* **768**, 12–17 (2017)

14. P. Ko, N. Nagata, Y. Tang, Hidden charged dark matter and chiral dark radiation. *Phys. Lett. B* **773**, 513–520 (2017)
15. A. Gomez-Valent, J. Sola, Relaxing the σ_8 -tension through running vacuum in the Universe. *EPL* **120**(3), 39001 (2017)
16. A. Gómez-Valent, J. Solà Peracaula, Density perturbations for running vacuum: a successful approach to structure formation and to the σ_8 -tension. *Mon. Not. Roy. Astron. Soc.* **478**(1), 126–145 (2018)
17. J. Ooba, B. Ratra, N. Sugiyama, Planck 2015 constraints on spatially-flat dynamical dark energy models (2018). [arXiv:1802.05571](https://arxiv.org/abs/1802.05571)
18. L. Kazantzidis, L. Perivolaropoulos, Evolution of the $f\sigma_8$ tension with Planck15/ Λ CDM and implications for modified gravity theories. *Phys. Rev. D* **97**(10), 103503 (2018)
19. Z. Sakr, S. Ilić, A. Blanchard, J. Bittar, W. Farah, Cluster counts: calibration issue or new physics? *Astron. Astrophys.* **620**, A78 (2018)
20. S. Kumar, R.C. Nunes, Echo of interactions in the dark sector. *Phys. Rev. D* **96**(10), 103511 (2017)
21. E. Di Valentino, A. Melchiorri, J. Silk, Cosmological hints of modified gravity? *Phys. Rev. D* **93**(2), 023513 (2016)
22. A.G. Riess, L. Macri, S. Casertano, H. Lampeitl, H.C. Ferguson, A.V. Filippenko, S.W. Jha, W. Li, R. Chornock, A 3% solution: determination of the Hubble constant with the Hubble space telescope and wide field camera 3. *Astrophys. J.* **730**, 119 (2011)
23. R.A. Battye, A. Moss, Evidence for massive neutrinos from cosmic microwave background and lensing observations. *Phys. Rev. Lett.* **112**(5), 051303 (2014)
24. E. Di Valentino, C. Boehm, E. Hivon, F.R. Bouchet, Reducing the H_0 and σ_8 tensions with Dark Matter-neutrino interactions. *Phys. Rev. D* **97**(4), 043513 (2018)
25. G.-B. Zhao, Dynamical dark energy in light of the latest observations. *Nat. Astron.* **1**(9), 627–632 (2017)
26. E. Di Valentino, A. Melchiorri, J. Silk, Reconciling Planck with the local value of H_0 in extended parameter space. *Phys. Lett. B* **761**, 242–246 (2016)
27. E. Di Valentino, A. Melchiorri, J. Silk, Beyond six parameters: extending Λ CDM. *Phys. Rev. D* **92**(12), 121302 (2015)
28. E. Di Valentino, A. Melchiorri, E.V. Linder, J. Silk, Constraining dark energy dynamics in extended parameter space. *Phys. Rev. D* **96**(2), 023523 (2017)
29. S. Anand, P. Chabul, A. Mazumdar, S. Mohanty, Cosmic viscosity as a remedy for tension between PLANCK and LSS data. *JCAP* **1711**(11), 005 (2017)
30. S. Anand, P. Chabul, A. Mazumdar, S. Mohanty, P. Parashari, Bounds on neutrino mass in viscous cosmology *JCAP* **1805**(05), 031 (2018)
31. H. Motohashi, A.A. Starobinsky, J. Yokoyama, Cosmology based on $f(R)$ gravity admits 1 eV sterile neutrinos. *Phys. Rev. Lett.* **110**(12), 121302 (2013)
32. S. Vagnozzi, E. Giusarma, O. Mena, K. Freese, M. Gerbino, S. Ho, M. Lattanzi, Unveiling ν secrets with cosmological data: neutrino masses and mass hierarchy. *Phys. Rev. D* **96**(12), 123503 (2017)
33. S. Vagnozzi, S. Dhawan, M. Gerbino, K. Freese, A. Goobar, O. Mena, Constraints on the sum of the neutrino masses in dynamical dark energy models with $w(z) \geq -1$ are tighter than those obtained in Λ CDM. *Phys. Rev. D* **98**(8), 083501 (2018)
34. S.R. Choudhury, A. Naskar, Bounds on sum of neutrino masses in a 12 parameter extended scenario with non-phantom dynamical dark energy ($w(z) \geq -1$) (2018). [arXiv:1807.02860](https://arxiv.org/abs/1807.02860)
35. S.R. Choudhury, S. Choubey, Updated bounds on sum of neutrino masses in various cosmological scenarios. *JCAP* **1809**(09), 017 (2018)
36. H. Wayne, I. Sawicki, Models of $f(R)$ cosmic acceleration that evade solar-system tests. *Phys. Rev. D* **76**, 064004 (2007)
37. J. Dosssett, H. Bin, D. Parkinson, Constraining models of $f(R)$ gravity with Planck and WiggleZ power spectrum data. *JCAP* **1403**, 046 (2014)
38. H. Bin, M. Raveri, M. Rizzato, A. Silvestri, Testing Hu-Sawicki $f(R)$ gravity with the effective field theory approach. *Mon. Not. R. Astron. Soc.* **459**(4), 3880–3889 (2016)
39. C. Brans, R.H. Dicke, Mach's principle and a relativistic theory of gravitation. *Phys. Rev.* **124**, 925–935 (1961)
40. D. Lovelock, The einstein tensor and its generalizations. *J. Math. Phys.* **12**(3), 498–501 (1971)
41. V.A. Kostelecky, Gravity, lorentz violation, and the standard model. *Phys. Rev. D* **69**, 105009 (2004)
42. J. Khoury, A. Weltman, Chameleon fields: awaiting surprises for tests of gravity in space. *Phys. Rev. Lett.* **93**, 171104 (2004)
43. P. Brax, A.-C. Davis, B. Li, H.A. Winther, A unified description of screened modified gravity. *Phys. Rev. D* **86**, 044015 (2012)
44. P. Brax, A.-C. Davis, B. Li, Modified gravity tomography. *Phys. Lett. B* **715**, 38–43 (2012)
45. S. Nojiri, S.D. Odintsov, Unified cosmic history in modified gravity: from $F(R)$ theory to Lorentz non-invariant models. *Phys. Rept.* **505**, 59–144 (2011)
46. A. De Felice, S. Tsujikawa, $f(R)$ theories. *Living Rev. Rel.* **13**, 3 (2010)
47. S. Nojiri, S.D. Odintsov, V.K. Oikonomou, Modified gravity theories on a nutshell: inflation, bounce and late-time evolution. *Phys. Rept.* **692**, 1–104 (2017)
48. T.P. Sotiriou, $f(R)$ gravity and scalar-tensor theory. *Class. Quant. Gravit.* **23**, 5117–5128 (2006)
49. P. Brax, P. Valageas, Impact on the power spectrum of screening in modified gravity scenarios. *Phys. Rev. D* **88**(2), 023527 (2013)
50. G.-B. Zhao, L. Pogosian, A. Silvestri, J. Zylberberg, Searching for modified growth patterns with tomographic surveys. *Phys. Rev. D* **79**, 083513 (2009)
51. A. Hojjati, L. Pogosian, G.-B. Zhao, Testing gravity with CAMB and CosmoMC. *JCAP* **1108**, 005 (2011)
52. Y.S. Song, W. Hu, I. Sawicki, The large scale structure of $f(R)$ gravity. *Phys. Rev. D* **75**, 044004 (2007)
53. E. Bertschinger, On the growth of perturbations as a test of dark energy. *Astrophys. J.* **648**, 797–806 (2006)
54. P. Zhang, Testing $f(R)$ gravity against the large scale structure of the universe. *Phys. Rev. D* **73**, 123504 (2006)
55. A.G. Riess, Observational evidence from supernovae for an accelerating universe and a cosmological constant. *Astron. J.* **116**, 1009–1038 (1998)
56. S. Perlmutter, Measurements of Omega and Lambda from 42 high redshift supernovae. *Astrophys. J.* **517**, 565–586 (1999)
57. D.M. Scolnic, The complete light-curve sample of spectroscopically confirmed SNe Ia from Pan-STARRS1 and cosmological constraints from the combined pantheon sample. *Astrophys. J.* **859**(2), 101 (2018)
58. L.H. Ford, Cosmological-constant damping by unstable scalar fields. *Phys. Rev. D* **35**, 2339–2344 (1987)
59. B. Ratra, P.J.E. Peebles, Cosmological consequences of a rolling homogeneous scalar field. *Phys. Rev. D* **37**, 3406–3427 (1988)
60. T. Chiba, N. Sugiyama, T. Nakamura, Cosmology with x matter. *Mon. Not. R. Astron. Soc.* **289**, L5–L9 (1997)
61. R.J.F. Marcondes, Interacting dark energy models in cosmology and large-scale structure observational tests. PhD thesis (2016)
62. M. Chevallier, D. Polarski, Accelerating universes with scaling dark matter. *Int. J. Mod. Phys. D* **10**, 213–224 (2001)
63. E.V. Linder, Exploring the expansion history of the universe. *Phys. Rev. Lett.* **90**, 091301 (2003)
64. E.M. Barboza Jr., J.S. Alcaniz, A parametric model for dark energy. *Phys. Lett. B* **666**, 415–419 (2008)

65. H.K. Jassal, J.S. Bagla, T. Padmanabhan, Understanding the origin of CMB constraints on dark energy. *Mon. Not. R. Astron. Soc.* **405**, 2639–2650 (2010)
66. C. Wetterich, Phenomenological parameterization of quintessence. *Phys. Lett. B* **594**, 17–22 (2004)
67. Y. Fukuda, Evidence for oscillation of atmospheric neutrinos. *Phys. Rev. Lett.* **81**, 1562–1567 (1998)
68. Q.R. Ahmad, Measurement of the rate of $\nu_e + d \rightarrow p + p + e^-$ interactions produced by 8B solar neutrinos at the Sudbury Neutrino Observatory. *Phys. Rev. Lett.* **87**, 071301 (2001)
69. J. Lesgourgues, S. Pastor, Massive neutrinos and cosmology. *Phys. Rept.* **429**, 307–379 (2006)
70. J. Lesgourgues, G. Mangano, G. Miele, S. Pastor, *Neutrino Cosmology* (Cambridge University Press, Cambridge, 2013)
71. P.F. de Salas, S. Pastor, Relic neutrino decoupling with flavour oscillations revisited. *JCAP* **1607**(07), 051 (2016)
72. N. Aghanim et al., Planck 2018 results VI. Cosmological parameters (2018). [arXiv:1807.06209](https://arxiv.org/abs/1807.06209)
73. C.-P. Ma, E. Bertschinger, Cosmological perturbation theory in the synchronous and conformal Newtonian gauges. *Astrophys. J.* **455**, 7–25 (1995)
74. A. Lewis, A. Challinor, A. Lasenby, Efficient computation of CMB anisotropies in closed FRW models. *Astrophys. J.* **538**, 473–476 (2000)
75. F. Beutler, C. Blake, M. Colless, D.H. Jones, L. Staveley-Smith, L. Campbell, Q. Parker, W. Saunders, F. Watson, The 6dF Galaxy survey: Baryon acoustic oscillations and the local Hubble Constant. *Mon. Not. R. Astron. Soc.* **416**, 3017–3032 (2011)
76. L. Anderson, The clustering of galaxies in the SDSS-III Baryon oscillation spectroscopic survey: baryon acoustic oscillations in the data releases 10 and 11 Galaxy samples. *Mon. Not. R. Astron. Soc.* **441**(1), 24–62 (2014)
77. A. Font-Ribera, Quasar-Lyman α forest cross-correlation from BOSS DR11: Baryon acoustic oscillations. *JCAP* **1405**, 027 (2014)
78. A.J. Ross, L. Samushia, C. Howlett, W.J. Percival, A. Burden, M. Manera, The clustering of the SDSS DR7 main Galaxy sample—I. A 4 per cent distance measure at $z = 0.15$. *Mon. Not. R. Astron. Soc.*, **449**(1), 835–847 (2015)
79. P.A.R. Ade et al. Planck 2013 results. XX. Cosmology from Sunyaev–Zeldovich cluster counts. *Astron. Astrophys.* **571**, A20 (2014)
80. M. Kilbinger, CFHTLenS: combined probe cosmological model comparison using 2D weak gravitational lensing. *Mon. Not. R. Astron. Soc.* **430**, 2200–2220 (2013)
81. C. Heymans, CFHTLenS tomographic weak lensing cosmological parameter constraints: mitigating the impact of intrinsic galaxy alignments. *Mon. Not. R. Astron. Soc.* **432**, 2433 (2013)
82. P.A.R. Ade et al, Planck 2013 results. XVII. Gravitational lensing by large-scale structure. *Astron. Astrophys.* **571**, A17 (2014)
83. K.K. Schaffer, The first public release of south pole telescope data: maps of a 95-square-degree field from 2008 observations. *Astrophys. J.* **743**, 90 (2011)
84. A. van Engelen, A measurement of gravitational lensing of the microwave background using South Pole Telescope data. *Astrophys. J.* **756**, 142 (2012)
85. F. Beutler, The clustering of galaxies in the SDSS-III baryon oscillation spectroscopic survey: testing gravity with redshift-space distortions using the power spectrum multipoles. *Mon. Not. R. Astron. Soc.* **443**(2), 1065–1089 (2014)
86. A. Lewis, S. Bridle, Cosmological parameters from CMB and other data: a Monte Carlo approach. *Phys. Rev. D* **66**, 103511 (2002)